Supporting Information

For the manuscript:
Solid-State NMR Structure Determination from Diagonal-Compensated, Sparsely Nonuniform-Sampled 4D Proton-Proton Restraints

By Rasmus Linser, Benjamin Bardiaux, Loren B. Andreas, Sven G. Hyberts, Vanessa K. Morris, Guido Pintacuda, Margaret Sunde, Ann H. Kwan, and Gerhard Wagner

Experimental (additions to the main manuscript)

In a time-shared 4D experiment, methyl resonances in indirect heteronuclear dimensions can be separated from the amide signals by their corresponding proton chemical shift if the indirect ^{1}H spectral width is large enough to avoid folding (here 12 ppm). In this case, ^{13}C and ^{15}N resonances may overlap, meaning that the carrier of indirect ^{15}N/^{13}C dimensions can both be set to the center of their respective ^{15}N/^{13}C bulk signal and the spectral width does not have to be increased with respect to non-time-shared acquisition. For 3D spectra, the single dimension (where no evolution of the scalar-coupled spin of the same group is exerted) has to ensure a separation of amide and methyl signals. Thus, in the case of a sole heteronuclear dimension, the spectral width has to be widened and the ^{15}N/^{13}C carrier frequencies be shifted to opposite ends of their respective bulk signal.

For assignment of the hydrophobin rodlets, a set of six dipolar-based backbone experiments (HNCA, HNCOCA, HNCACB, HNCOCACB, HNCO, HNCACO)[1,2] were recorded at 800 MHz ^{1}H Larmor frequency on the same sample as described in the main manuscript. The temperature and MAS settings were identical as described there. Spectra were analysed in CCPNmr.

Methyl signals with residual protonation

Unambiguous ^{1}H-^{1}H correlations are also of utmost benefit for the assignment of backbone amide and side chain methyl (or in the case of sparse aliphatic protonation also for other aliphatic) proton/carbon resonance sets. This again is particularly interesting in all those cases where limited resolution leads to ambiguities in the assignment process. Even though not used here, labeling schemes enabling quantitative methyl protonation or sparsely protonated aliphatic side chains have been reported elsewhere and are straightforward to implement. For natural-abundance methyl protonation, correlations involving methyls are only weak in the 4D spectra. This is true even though the more

sensitive 2D and 3D correlations exploiting the time-shared approach prove the enormous potency of including methyl-group-associated coherences. Methyl data reported in Main Manuscript Figure 5 for comparison of structures with and without methyl restraints were thus taken from an experiment using the truncated (3D) scheme of the pulse sequence with higher sensitivity. Supplementary Figure 1 A) displays signal intensities for amide and methyl bulk in the first increment of an RFDR experiment with "natural abundance" methyl protonation. B) shows a cross peak between K27 H^N and M25^{met}, representative for the weak intensity of the obtained methyl-amid cross peaks in the 4D with "natural abundance" protonation. Due to the effective $^1H^{met}$ dilution to only ~ 9%, methyl-methyl cross peaks are not expected to be observed with the "natural-abundance" protonation used here in any spectrum. Even though the potency of time-shared spectra is becoming obvious, a higher aliphatic protonation would clearly facilitate the full exploitation of this concept.

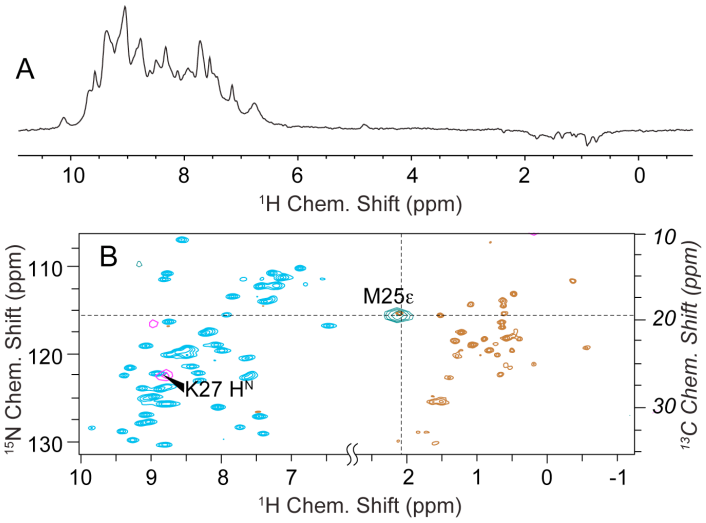

Supplementary Figure 1: A) First transient (128 scans) for visualization of amide and methyl bulk signal intensity obtained using 97% ^{2}H-/99% ^{13}C-labeled glucose (corresponding to ~9% methyl protonation) and $^1H^N$ back-exchange of 25%. **B)** Also in the 4D, cross peaks involving methyl groups are already well visible due to the residual methyl proton labeling. This is depicted here for magnetization transfer between M25ε and K27 H^N, at F1 and F2 chemical shifts of 2.0 and 115.4 ppm (corresponding to 19.0 ppm ^{13}C chemical shift), respectively, as marked by dashed lines. Positive and negative levels of the 4D spectrum are drawn in green and magenta, respectively, whereas the reference 2D time-shared HN/C correlation, which is overlaid for better overview, is drawn in blue and brown for positive and negative contours, respectively. These correlations are known to be of much benefit for structure-relevant data sets. As a straightforward improvement in future studies, however, the use of RAP[3] or methyl-labeled protein[4,5] is expected to generate maximum methyl-amide and methyl-methyl cross peak quality. The ^{15}N shifts are translated into the corresponding ^{13}C values on the right. Both A) and B) show spectra recorded on the SH3 domain of α-spectrin.

Spinning-side-band reduction

In solid-state homonuclear correlations, strong auto-correlation signals can be associated with immense spinning sidebands in indirect dimensions. Even at highest spinning frequencies technically achievable to-date this can be a major problem, particularly at higher B_0 fields. Spectral widths in indirect dimensions are usually adjusted in such a way that they provide sufficient space for isolated side bands. Due to time constraints, however, this is difficult or even impossible upon multi-dimensional recording. Here, such strong sidebands from autocorrelation signals and the associated artifacts are automatically eliminated by diagonal-signal compensation, since their intensity would be directly proportional to their respective (suppressed) diagonal signals. Comparison of Supplementary Figures 2A and B shows the significant effects for a time-shared 2D plane. The elimination of auto-correlation side bands is particularly beneficial in time-shared experiments due to the large separation of amide-methyl cross peaks from the diagonal. Methyl-to-amide cross peaks are even more susceptible to deterioration by strong diagonal peaks when samples with low methyl protonation are considered. This is the case for proteins without specific ILV methyl labeling, as they are used in our study here.

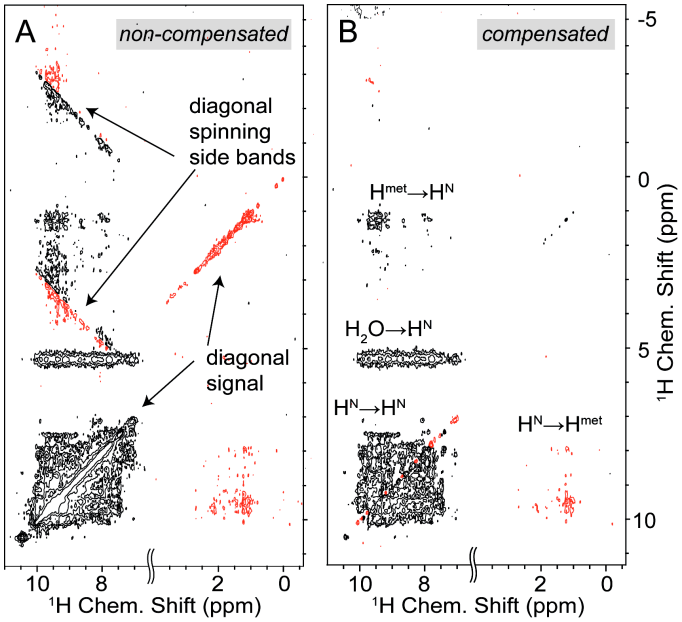

Supplementary Figure 2: Compensation of diagonal signal. **A)** First-2D time-shared $^1H/^1H$ spectra of non-diagonal-free and **(B)** diagonal-free experiments, demonstrating the yield of $H^N\rightarrow H^N$, $H^N\rightarrow H^{met}$ and $H^{met}\rightarrow H^N$ cross peaks as well as the advantageous cancelation of aliased MAS spinning side bands in indirect dimensions. Spinning-side-band cancelation is particularly helpful at higher B_0 fields and in time-shared experiments, which require larger spectral widths in indirect dimensions and make suitable placement of folded side bands disadvantageous. The spectra were recorded on the SH3 domain as 2D spectra with 14 ms indirect ^{1}H evolution time at 25 kHz MAS. Black and red contours represent positive and negative peaks, respectively.

Sensitivity considerations

The sensitivity retained with diagonal suppression depends on the relative diagonal intensity in the regular and compensating spectra. A relative superiority of compensation-scan intensity naturally depends on the length of the mixing step. For longer mixing times, performance of regular scans decreases due to rf-inhomogeneity and pulse imperfections in the mixing sequence. In addition to the overall loss of magnetization during mixing, as derived from the decreasing bulk-amide signal, intensity is redistributed from the diagonal peak towards cross peaks. This is the cause of cross peak buildup (see Supplementary Figure 3) and naturally reduces diagonal peak intensities further. The effect is expected to be dependent on the local environment of each spin, including the local proton density and dynamics of the spins involved in the magnetization transfer, and thus represents a residue-specific factor.

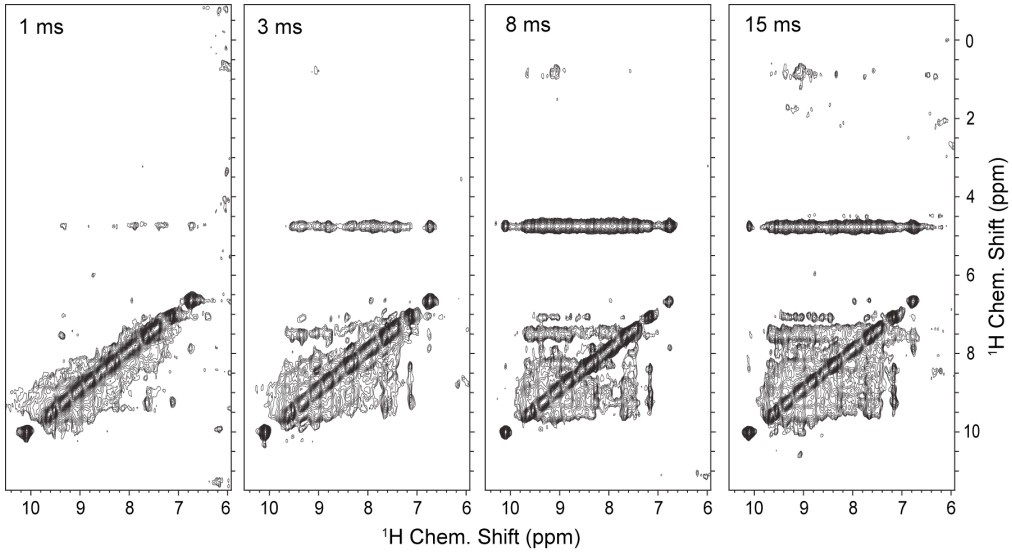

Supplementary Figure 3: Buildup of cross peak intensity upon dipolar mixing. Proton/proton correlations in solid-state NMR on partially deuterated samples are a versatile additional source of distance information. Successive spectra depict mixing times of 1, 3, 8, and 15 ms. Similar as in solution,[6] the buildup of cross peak intensity is associated with both, decreasing diagonal intensity and loss of overall magnetization. Spectra were recorded at 600 MHz Larmor frequency using the SH3 domain of α-spectrin with a maximum indirect evolution period of 8.3 ms using RFDR with 20-ppm indirect spectral width.

Implementation with increasing ratios between the numbers of regular and diagonal-compensating transients, however, requires acquisition of a larger total number of scans. This can turn into total-acquisition-time-related problems for high-dimensionality spectra or large spectral widths. For practical reasons, the actual ratio between main scans and compensation scans will reflect a compromise between these aspects and may involve additional downscaling of the compensation transients rather than further increase of the ratio between regular and compensation scans.

Using 2 out of 3 scans for cross-peak-containing scans, as described in the main manuscript for SH3, the cross-peak *signal* is reduced to 2/3 in comparison to what it would be in a non-compensated experiment. The *noise* introduced upon Fourier

transformation of the sum after scaling of the compensation scan to 0.75 is reduced to $\frac{\sqrt{2+0.75^2}}{\sqrt{3}}$. Together, this yields approximately 72% of the cross-peak signal to noise compared to a non-compensated experiment. For hydrophobin, application of 4 regular scans for each compensating scan scaled to 0.6 results in signal-to-noise of approximately 86% of that obtained from a non compensated experiment recorded in the same amount of time. In both cases, this sensitivity is significantly larger than in approaches with a 1:1 compensation as proposed for subtraction in solution, which sacrifices 50% of the signal for cleaning up.[7] Coherence selection in terms of TROSY-NOESY-TROSY[8] is associated with a 50% sacrifice of all magnetization in the first block (necessary for the initial selection of the TROSY component) in addition to another 50% sacrifice for diagonal compensation. Moreover, scalar sequences, particularly those with prolonged ^{15}N transverse relaxation times like the latter, would be associated with devastating losses during transfers for most samples if applied in solid-state NMR. Both techniques would thus make the concept of ^{1}H-^{1}H distance measurements practically impossible.

In general, for a given experimental setup, the factor $\alpha(x)$ reducing uncompensated signal-to-noise upon diagonal compensation in our case is:

$$\alpha(x) = \frac{x}{\sqrt{x + S_F^2 \frac{x^2}{1-x}}},$$

where x is the fraction of recorded scans with mixing out of the number of total scans recorded. S_F is the scaling factor (how much the compensating spectrum is scaled down to match the regular spectrum in the case when both have equal scans).

As it results from setting the first derivative $\frac{\partial \alpha(x)}{\partial x} = 0$, optimal sensitivity is achieved for:

$$x_{opt} = \frac{1}{S_F + 1}.$$

For this optimal fraction, the factor $\alpha(x_{opt})$ becomes

$$\alpha_{opt} = \frac{1}{S_F + 1}.$$

This is the optimal sensitivity remaining with diagonal compensation. It is 0.870 for hydrophobin (100 % ^{1}H backexchange at 60 kHz MAS), and 0.727 for SH3 (25 % backexchange at 25 kHz MAS), using the scaling factors reported in the text of S_F = 0.15 (downscaling of 1 compensation scan to 0.6 to match the sum of 4 regular scans), and 0.375 (downscaling of 1 compensation scan to 0.75 to match the sum of 2 regular scans), respectively.

Despite the need for further downscaling after recording the experiments, the obtained sensitivity factors are very similar to the theoretical optimum. As can also be seen in the plot in Supplementary Figure 4, the obtained signal-to-noise is not very sensitive to small missets of the ratio x.

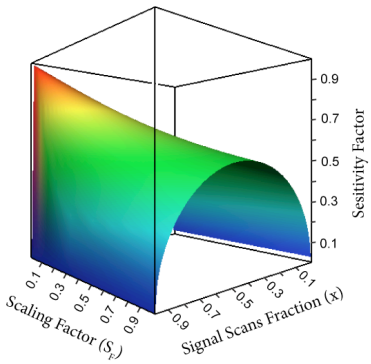

Supplementary Figure 4: Remaining sensitivity for different x and S_F combinations. (x is the fraction of cross-peaks-containing scans out of the total scans recorded, S_F is the scaling required to compensate a diagonal signal for spectra recorded with a 1:1 ratio of regular scans to compensation scans.

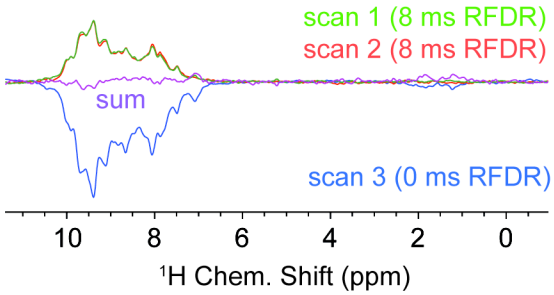

Supplementary Figure 5: In contrast to NOESY experiments in solution, dipolar mixing suffers from pulse imperfections during mixing in regular scans, concomitantly requiring a lower number of compensation scans when diagonal-free spectra are pursued. The plot shows the bulk signal in successive first scans 1, 2, and 3 and their sum (here without further scaling) in a triple of transients applied to the SH3 domain at 25 % proton backexchange. Even though a ratio of 1 compensation scan out of 3 scans in total seems adequate from looking at the bulk (reflecting overall signal loss during mixing), diagonal compensation needs even lower ratios (or downscaling of the compensation scan, if the resolution limits within a given time are reached) due to redistribution of magnetization from the diagonal to cross peaks.

Considerations valid for 4D spectra

Undistorted NUS 4D spectra are the current state-of-the-art approach for unambiguous assignment of spatial contacts in the solution state. In the solid state, these methods correlate protons with the potential resolution obtained in the fingerprint HN spectra, but also provide unambiguous evidence for ^{1}H-^{1}H proximities with distances of up to >10 Å.[9] An additional advantage towards a high reliability of the data is that correlations found for A→B can be reconfirmed by cross peaks B→A, similar to heteronuclear-edited 3D experiments. In addition, in 4D correlations, matching peaks can easily be found in the same manner on the basis of *F1*/*F2* planes or *F3*/*F4* planes, as depicted in Supplementary Figure 6.

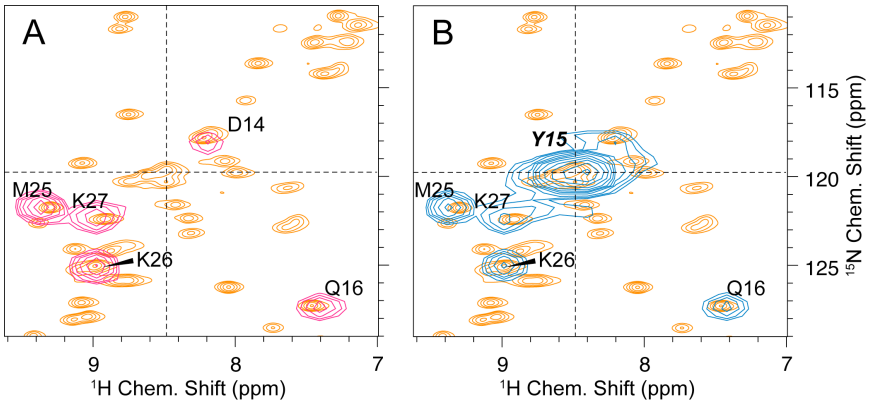

Supplementary Figure 6: Bidirectionality of magnetization transfer. Rather than finding correlations in *F3*/*F4* cross planes (like in Figures 2A and B of the Main Manuscript), an identical information content is displayed when looking at *F1*(^{1}H)/*F2*(^{15}N) planes. This is depicted here for residues in the vicinity of Y15 in the SH3 domain. Like in Figures 2A and B of the Main Manuscript, frames **A)** and **B)** here depict diagonal-compensated and non-compensated cross planes from the 4D experiment, respectively. The two directions of magnetization transfer between sites can be used for reconfirmation and higher accuracy of the restraints extracted. In all slices the reference 2D HN correlation (yellow) is overlaid for better overview. Dashed lines indicate the positions of the ^{1}H and ^{15}N shift used in the dimensions perpendicular to the paper plane.

Structure calculation

After combining information from peak pairs reflecting the same restraint by simple averaging, 4D-cross-peak volumes were normalized by dividing by the 2D peak volumes of both residues connected as found in a 2D H/N correlation. Out of 103 non-redundant restraints, a total of four were discarded for calibration, structure calculation and analysis (three corresponding to inter-molecular cross-peaks in the crystal lattice and one being a wrong assignment). Calibrated distance restraints were derived from the intensity I_{ij} of a normalized cross peak between atom i and j using a uniform calibration procedure. The calibration was carried out using the following relationship:

$$I_{ij} = kd_{ij}^{-3}$$

with the calibration factor k:

$$k = \frac{\langle I_{ij} \rangle}{\langle d_{ij} \rangle^{-3}}$$

Without prior knowledge of the distances, $\langle d_{ij} \rangle$ was chosen to be 4.0 Å. Using this initial calibration, a first structure calculation was performed and the resulting distances d_{ij} served for the second and final calibration.

Structure ensembles were calculated with CNS[10] using the simulated protocols from ARIA 2.3.[11] For the initial calibration, 100 conformers were calculated and the 10 lowest-energy ones were used to perform the second calibration.
For the final calculation with calibrated distances, 200 conformers were generated and the 10 lowest-energy ones were refined in a shell of water molecules and analyzed.

For all structure calculations, a log-harmonic energy potential[12] was employed for the distance restraints. This potential allows a better application of the distance restraints through a single energy minimum (the calibrated distance) and an automated estimation of the optimal weight on the distance restraints.

In addition, backbone dihedral angle restraints predicted by TALOS+[13] from backbone chemical shifts were used in the structure calculation.

Rather than specific restraints, distance classes still seem the better choice to accommodate intensity-distance deviations. Nevertheless, the actual peak intensity of correctly identified peaks results to be an important feature for facilitated structure calculations. We compared the final calibrated distances with the corresponding distances in the X-ray structure (2NUZ). Considering that factors like local dynamics and relaxation properties generally cause inevitable variations for the individual NMR-peak integrals, the overall accuracy, at least in the case of diagonal compensation, seems indeed much higher than reported for traditional spin-diffusion experiments.[14,15] Normalization procedures taking residue-specific parameters, like local relaxation properties, into account could be thought as further increasing the accuracy of the distance restraints.

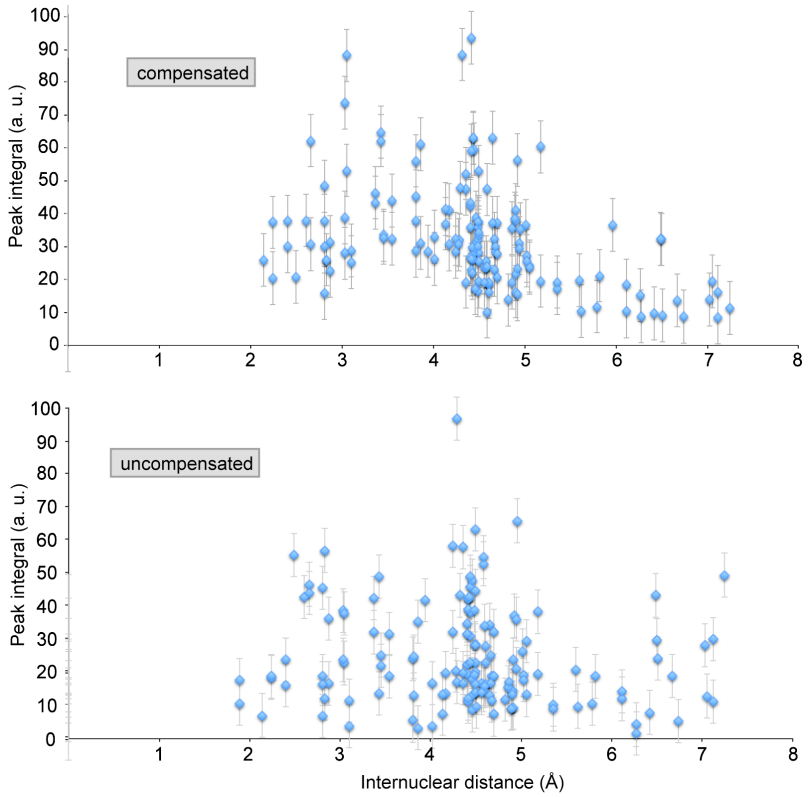

Supplementary Figure 7: Correlation between amide-amide peak integrals and the corresponding distances in the X-ray structure 2NUZ. Peaks were picked at identical positions with subtraction of the diagonal-only transients (compensated, above) and without (uncompensated, below). Error bars shown represent the level of signal to noise obtained in the spectra.

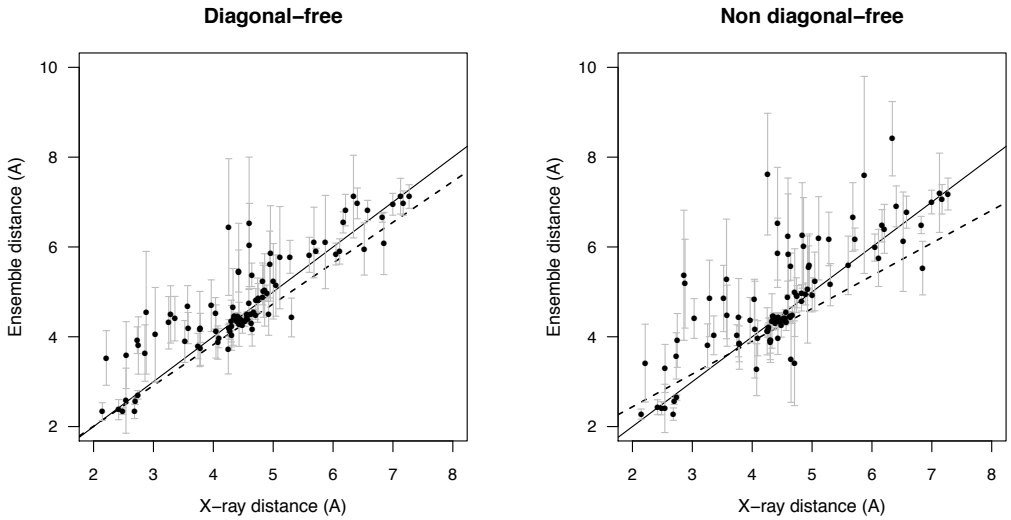

Supplementary Figure 8: Correlation between the distances in the X-ray structure and the corresponding average distances in the structure ensembles for the non-redundant H-H restraints. Standard deviations of distances in the structure ensemble are plotted with grey bars. The diagonal and the linear regression fit are shown in plain and dotted lines, respectively.

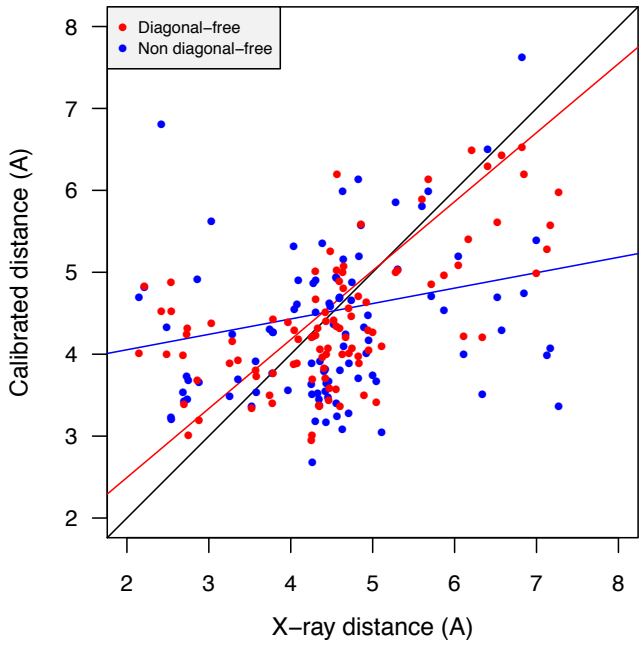

Supplementary Figure 9: Correlation between the calibrated distances and the corresponding distances in the X-ray structure. The diagonal (black) and the linear regression fit for diagonal-free (red, correlation coefficient of 0.59) and non-diagonal-free (blue, correlation coefficient of 0.27) are shown in plain lines.

	Distance accuracy		Ensemble Precision (Å)		Bias to X-ray (Å)	
Experiment	**Corr. coeff.**	**RMSD (A)**	**backbone**	**all atoms**	**backbone**	**all atoms**
Compensated	0.59	0.96	1.28 ± 0.21	2.05 ± 0.28	1.69	2.59
Uncompensated	0.27	1.79	1.39 ± 0.34	2.28 ± 0.43	2.05	3.03

Supplementary Figure 10: Correlation coefficients (Pearson) and RMSD between calibrated distances (before structure calculation) and the corresponding X-ray distances, as well as structure ensemble statistics (10 best conformers analyzed). "all atoms" RMSDs refer to the non-hydrogen atoms only and ignore the N-terminus and tip of the RT loop, which are known to be highly flexible.[16]

Effects for heterogeneous structures

Broad peaks in solid-state NMR spectra can be a consequence of structural heterogeneity or of homogeneous line broadening. Both factors can be representative of important biochemical properties of the molecules being studied and are expected for heterogeneous and dynamic ensembles. These are common and widespread features in many natural substances.[17-19] Cases in which they impede studies of scientific interest

include specimens in material sciences, in chemistry, and biological samples when subjected to low temperatures such as for Dynamic Nuclear Polarization techniques[20] and many amyloid-forming[21,22] or membrane-embedded proteins[23,24]. Prominent examples where poor molecular order limits solid-state NMR are non-crystalline samples of fibrils formed in the course of neurodegenerative diseases, such as Alzheimer's[25,26] and prion proteins[27]. They also include the functional hydrophobin amyloids (see Supplementary Figures 11 to 13 in addition to the main manuscript), which play a role in tailoring surface properties of fungal spores. Homogeneous line broadening can be associated with fibrillar exchange processes[28] or intra-membrane rotational diffusion[29] on the NMR time scale.

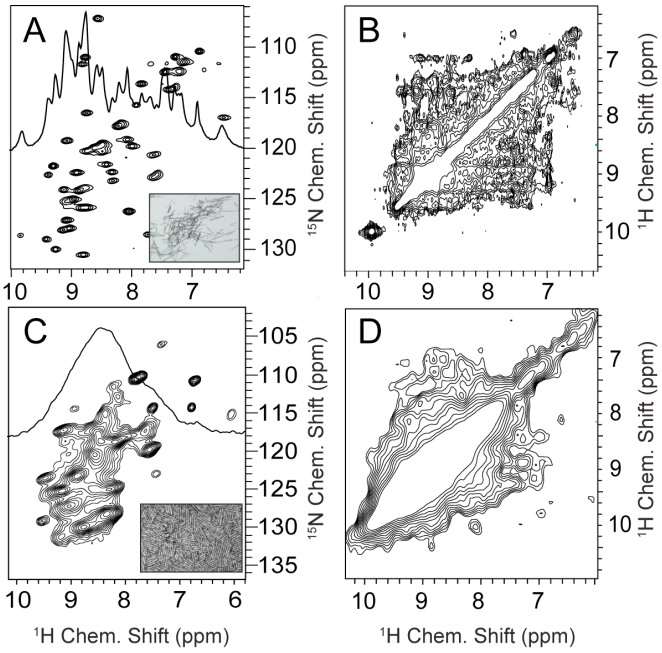

Supplementary Figure 11: Comparison of spectral quality for samples of high and low molecular order. Diagonal peaks in homonuclear correlations for excellent sample resolution and in case of low molecular order. Whereas an intense but sharp diagonal already leads to difficulties in assignment and quantification of peak intensities, broad autocorrelation signals can render spectral analysis impossible. The figure compares spectral resolution in heteronuclear (**A** and **C**) and homonuclear (**B** and **D**) correlation experiments of microcrystalline samples (**A** and **B**) and fibrillar preparations (**C** and **D**). ^{1}H-^{1}H correlations shown in **B** and **D** were recorded using 8 ms RFDR mixing. Indirect evolution times (14 ms and 5 ms, respectively) and processing (Gaussian multiplication of -10 Hz and a shift of the bell by 0.1 and exponential multiplication with 100 Hz, respectively) were chosen as adequate matches for the effective ^{1}H linewidths of the SH3 domain and hydrophobin rodlets as obtained in HN correlations (25-30 Hz and >250 Hz, respectively). (The width of the microscopic/electron-microscopic image inset of microcrystals and rodlets is 0.2 mm and 300 nm, respectively.) The hydrophobin data shown here accords to procedures also used for the SH3 domain using 25% proton backexchange at 25 kHz MAS and 700 MHz ^{1}H Larmor frequency.

Figure 12 shows application of diagonal compensation to a sample of the highly heterogeneous hydrophobin amyloids. Diagonal compensation in challenging samples

like these will not remove the difficulties related to a poor definition of peaks and resulting peak overlap completely. As it is predicted from Supplementary Figure 12, however, the approach turns an insolvable task into something well doable.

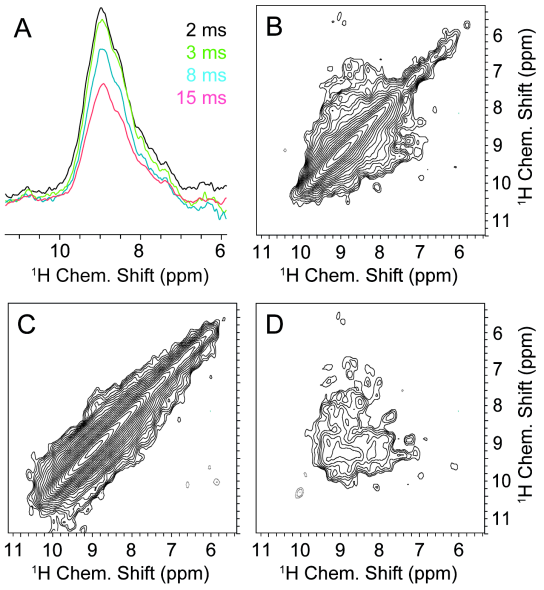

Supplementary Figure 12: Application of diagonal compensation to hydrophobin rodlets, a case of large sample heterogeneity. **A)** Decay of magnetization upon increasing mixing time. This general behavior, occurring similarly in the case of the micro-crystalline SH3, is shown here for a sample containing hydrophobin rodlets. **B-D)** Diagonal signal severely abrogates spectral quality of structural data in the presence of strong linebroadening, shown here for the first $^{1}H/^{1}H$ plane of a 4D experiment recorded on hydrophobin rodlets (with an effective recording time for each of the 2D planes as shown in **B** and **C** of 5 min, recorded as non-time-shared $^{1}H^{N}$-$^{1}H^{N}$ correlations using 5 ms indirect acquisition times and 100 Hz Gaussian multiplication as adequate matches to the lineshapes in 2D H/N correlations, see Figure 11). In this case, the diagonal-only spectrum (**C**) was scaled to 0.33 before subtraction from **B**) to yield **D)** as the diagonal-compensated spectrum. These spectra were recorded with a proton back-substitution of 25% at 700 MHz ^{1}H Larmor frequency.

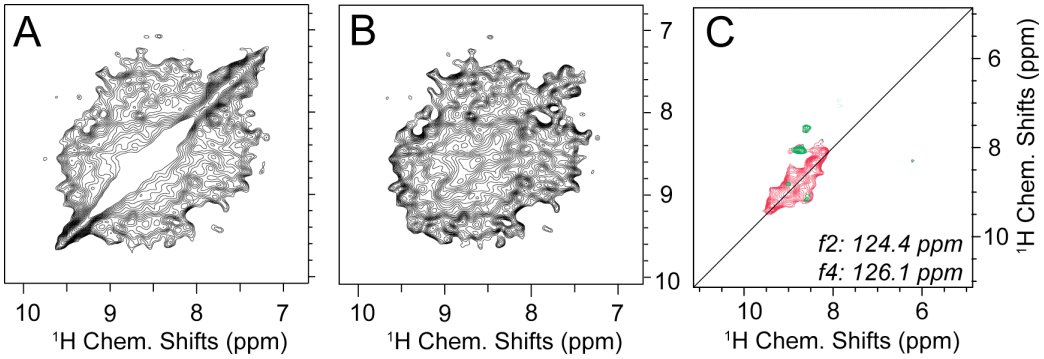

Supplementary Figure 13: Application of diagonal compensation to hydrophobins with a 100% proton back exchange at fast spinning. **A)** 2D correlation without and with **(B)** diagonal compensation. Both dimensions were truncated to 10 ms chemical shift evolution and apodized using Gaussian Multiplication with -10 Hz and shift of the bell by 0.05. The second plot was prepared using 1 out of 5 scans for

acquisition of diagonal compensation and further downscaling to 0.4 before subtraction. **C)** Representative 2D slice from a 4D like in Main-Text Figures 3E and F, but looking at dimensions f1(^{1}H)/f4(^{1}H) rather than f3(^{15}N)/f4(^{1}H). Magenta and green contours represent non-compensated and compensated spectra, respectively.
As expected for non-stochastic protonation, diagonal signal is less relative to cross peak intensity compared to stochastic protonation schemes. A lower number of compensation scans required, however, also reduces the cost of compensation, making it equally feasible for straightforward acquisition of high-quality data using single-quantum recoupling sequences. These spectra were recorded at 1 GHz ^{1}H Larmor frequency.

Supporting Information References:

(1) Knight, M. J.; Webber, A. L.; Pell, A. J.; Guerry, P.; Barbet-Massin, E.; Bertini, I.; Felli, I. C.; Gonnelli, L.; Pierattelli, R.; Emsley, L.; Lesage, A.; Herrmann, T.; Pintacuda, G. *Angew. Chem., Int. Ed.* **2011**, *50*, 11697.
(2) Marchetti, A.; Jehle, S.; Felletti, M.; Knight, M. J.; Wang, Y.; Xu, Z. Q.; Park, A. Y.; Otting, G.; Lesage, A.; Emsley, L.; Dixon, N. E.; Pintacuda, G. *Angew. Chem. Int. Ed.* **2012**, *51*, 10756.
(3) Asami, S.; Schmieder, P.; Reif, B. *J. Am. Chem. Soc.* **2010**, *132*, 15133.
(4) Agarwal, V.; Diehl, A.; Skrynnikov, N.; Reif, B. *J. Am. Chem. Soc.* **2006**, *128*, 12620.
(5) Huber, M.; Hiller, S.; Schanda, P.; Ernst, M.; Böckmann, A.; Verel, R.; Meier, B. H. *ChemPhysChem* **2011**, *12*, 915.
(6) Kumar, A.; Wagner, G.; Ernst, R. R.; Wüthrich, K. *J. Am. Chem. Soc.* **1981**, *103*, 3654.
(7) Denk, W.; Wagner, G.; Rance, M.; Wüthrich, K. *J. Magn. Reson.* **1985**, *62*, 350.
(8) Diercks, T.; Truffault, V.; Coles, M.; Millet, O. *J. Am. Chem. Soc.* **2010**, *132*, 2138.
(9) Linser, R.; Bardiaux, B.; Higman, V.; Fink, U.; Reif, B. *J. Am. Chem. Soc.* **2011**, *133*, 5905.
(10) Brünger, A. T.; Adams, P. D.; Clore, G. M.; DeLano, W. L.; Gros, P.; Grosse-Kunstleve, R. W.; Jiang, J. S.; Kuszewski, J. J.; Nilges, M.; Pannu, N. S.; Read, R. J.; Rice, L. M.; Simonson, T.; Warren, G. L. *Acta Crystallogr., Sect. D: Biol. Crystallogr.* **1998**, *54*, 905.
(11) Rieping, W.; Habeck, M.; Bardiaux, B.; Bernard, M.; Malliavin, T. E.; Nilges, M. *Bioinformatics* **2007**, *23*, 381.
(12) Nilges, M.; Bernard, A.; Bardiaux, B.; Malliavin, T. E.; Habeck, M.; Rieping, W. *Structure* **2008**, *16*, 1305.
(13) Shen, Y.; Delaglio, F.; Cornilescu, G.; Bax, A. *J. Biomol. NMR* **2009**, *44*, 213.
(14) Castellani, F.; van Rossum, B.-J.; Diehl, A.; Schubert, M.; Rehbein, K.; Oschkinat, H. *Nature* **2002**, *420*, 98.
(15) Loquet, A.; Bardiaux, B.; Gardiennet, C.; Blanchet, C.; Baldus, M.; Nilges, M.; Malliavin, T.; Böckmann, A. *J. Am. Chem. Soc.* **2008**, *130*, 3579.
(16) Linser, R.; Fink, U.; Reif, B. *J. Am. Chem. Soc.* **2010**, *132*, 8891.

(17) *Nat. Chem. Biol.* **2010**, *6*, 691.
(18) Altschuh, D.; Björkelund, H.; Strandgård, J.; Choulier, L.; Malmqvist, M.; Andersson, K. *Biochem. Biophys. Res. Commun.* **2012**, *428*, 74.
(19) Solomatin, S. V.; Greenfeld, M.; Herschlag, D. *Nat. Struct. Mol. Biol.* **2011**, *18*, 732.
(20) Linden, A.; Franks, W.; Akbey, Ü.; Lange, S.; Rossum, B.-J. v.; Oschkinat, H. *J. Biomol. NMR* **2011**, *51*, 283.
(21) Nielsen, J. T.; Bjerring, M.; Jeppesen, M. D.; Pedersen, R. O.; Pedersen, J. M.; Hein, K. L.; Vosegaard, T.; Skrydstrup, T.; Otzen, D. E.; Nielsen, N. C. *Angew. Chem., Int. Ed.* **2009**, *48*, 2118
(22) Comellas, G.; Lemkau, L. R.; Zhou, D. H.; George, J. M.; Rienstra, C. M. *J. Am. Chem. Soc.* **2012**, *134*, 5090.
(23) Linser, R.; Dasari, M.; Hiller, M.; Higman, V.; Fink, U.; Lopez del Amo, J.-M.; Markovic, S.; Handel, L.; Kessler, B.; Schmieder, P.; Oesterhelt, D.; Oschkinat, H.; Reif, B. *Angew. Chem., Int. Ed.* **2011**, *50*, 4508.
(24) Ward, M. E.; Shi, L.; Lake, E.; Krishnamurthy, S.; Hutchins, H.; Brown, L. S.; Ladizhansky, V. *J. Am. Chem. Soc.* **2011**, *133*, 17434.
(25) Paravastu, A. K.; Leapman, R. D.; Yau, W. M.; Tycko, R. *Proc. Natl. Acad. Sci. U.S.A.* **2008**, *47*, 18349.
(26) Lopez del Amo, J.-M.; Schmidt, M.; Fink, U.; Dasari, M.; Fändrich, M.; Reif, B. *Angew. Chem., Int. Ed.* **2012**, *51*, 6136.
(27) Helmus, J. J.; Surewicz, K.; Nadaud, P. S.; Surewicz, W. K.; Jaroniec, C. P. *Proc. Natl. Acad. Sci. USA* **2008**, *105*, 6284.
(28) Fawzi, N. L.; Ying, J.; Ghirlando, R.; Torchia, D. A.; Clore, G. M. *Nature* **2011**, *480*, 268.
(29) Park, S. H.; Mrse, A. A.; Nevzorov, A. A.; Angelis, A. A. D.; Opella, S. J. *J. Magn. Reson.* **2006**, *178*, 162.